Hindawi
Mathematical Problems in Engineering
Volume 2023, Article ID 9782470, 1 page
https://doi.org/10.1155/2023/9782470

Retraction

Retracted: AI Based Gravity Compensation Algorithm and Simulation of Load End of Robotic Arm Wrist Force

Mathematical Problems in Engineering

Received 18 July 2023; Accepted 18 July 2023; Published 19 July 2023

This article has been retracted by Hindawi following an investigation undertaken by the publisher [1]. This investigation has uncovered evidence of one or more of the following indicators of systematic manipulation of the publication process:

(1) Discrepancies in scope
(2) Discrepancies in the description of the research reported
(3) Discrepancies between the availability of data and the research described
(4) Inappropriate citations
(5) Incoherent, meaningless and/or irrelevant content included in the article
(6) Peer-review manipulation

The presence of these indicators undermines our confidence in the integrity of the article's content and we cannot, therefore, vouch for its reliability. Please note that this notice is intended solely to alert readers that the content of this article is unreliable. We have not investigated whether authors were aware of or involved in the systematic manipulation of the publication process.

Wiley and Hindawi regrets that the usual quality checks did not identify these issues before publication and have since put additional measures in place to safeguard research integrity.

We wish to credit our own Research Integrity and Research Publishing teams and anonymous and named external researchers and research integrity experts for contributing to this investigation.

The corresponding author, as the representative of all authors, has been given the opportunity to register their agreement or disagreement to this retraction. We have kept a record of any response received.

References

[1] L. Chen, H. Sun, W. Zhao, and T. Yu, "AI Based Gravity Compensation Algorithm and Simulation of Load End of Robotic Arm Wrist Force," *Mathematical Problems in Engineering*, vol. 2021, Article ID 5551544, 11 pages, 2021.

Hindawi
Mathematical Problems in Engineering
Volume 2021, Article ID 5551544, 11 pages
https://doi.org/10.1155/2021/5551544

Research Article

AI Based Gravity Compensation Algorithm and Simulation of Load End of Robotic Arm Wrist Force

Liang Chen,[1] **Hanxu Sun**,[1] **Wei Zhao**,[2] **and Tao Yu**[3]

[1]*School of Automation, Beijing University of Posts and Telecommunications, Beijing 10876, China*
[2]*School of Information Engineering, Beijing Institute of Graphic Communications, Beijing, China*
[3]*College of Mechanical Engineering and Automation, Liaoning University of Technology, Jinzhou, Liaoning, China*

Correspondence should be addressed to Liang Chen; chenliang968@bupt.edu.cn

Received 13 January 2021; Revised 3 February 2021; Accepted 23 February 2021; Published 5 March 2021

Academic Editor: Sang-Bing Tsai

With the rapid development of mechatronics and robotics technology, the application of robots has been extended from the industrial field to daily life and has become an indispensable part of work and daily life. The accuracy and flexibility of the operator determine the operating efficiency of the robot. Although the level of development of the operator is constantly improving, the traditional operator has a simple structure and generally adopts parallel movement or tightening. The holding structure has poor flexibility and stability, making it difficult to achieve precise position capture and control and cannot meet the requirements of delicate tasks. In this paper, a basic force analysis of the manipulator is carried out, and the change trend of the force and driving force of each joint when the manipulator is grasping objects is obtained, so as to determine that the manipulator can grasp the object stably; then, in the strength analysis of the manipulator, it is determined that the material meets the strength requirements. This paper conducts an output voltage experiment on the static performance and coupling error of the mechanical arm wrist force sensor. Secondly, in order to study the influence of the temperature change in the space environment on the zero-point output of the mechanical arm sensor, a high and low temperature test box are used to simulate the temperature brought by the temperature change to the sensor. Experiments show that the maximum coupling error of the sensor is 1.81%, which is less than 2% of the design index. This indicates that the operator sensor is used to detect the force and torque that the space operator's edge operator experiences when it interacts with the external environment and provides the necessary power sensing information for power control and compatible operator motion control, completing some complex; the Fine project is an important prerequisite for realizing the intelligence of space operators.

1. Introduction

As the requirements for refinement and intelligence of operation tasks continue to increase, mechanical arms that lack force perception will not be able to meet the requirements of operation tasks. Increasing the force-sensing ability on the robotic arm is an important functional requirement and development trend of the robotic arm. Manipulator wrist force sensor is one of the most important multidimensional power sensors for robots. It is a power sensor with two ends connected to the robot wrist and claws. When the robot arm tightens the workpiece for operation, it can measure the robot arm and the external environment. According to the concept and characteristics of supply chain integration, the relevant factors that influence the methods of evaluation and evaluation of business performance determine the supply chain integration and the indicators of measuring the performance of companies and define relevant models. This document uses the existing data from listed companies in the software services and information technology industry to separate supply chain integration into customer integration and supplier integration, exploring the relationship between customer integration, vendor integration, and corporate performance.

Relying on its advanced software and hardware platforms, computer vision technology, and motion control technology, foreign countries have always been in a leading position in the field of wrist force sensor research. In recent

years, dozens of wrist force sensor products or prototypes have been developed. Sprowl analyzed the relationship between the influence of the gravity level disturbance on the inertial navigation system and the maneuvering mode of the carrier. The gravity level disturbance signal caused by the vertical deviation is a distance-related signal. The maneuvering mode of the carrier determines the distance-related signal to time elated signal conversion method [1]. Ahlin et al. quantitatively analyzed the influence of vertical deviation on inertial navigation based on the single-channel error covariance model of inertial navigation [2]. Cuervo proposed that the attitude error and velocity error caused by the vertical deviation in the Schuler ring have different frequency domain characteristics, and the grid resolution required for the compensation attitude calculation and velocity calculation is different [3]. Farman et al. discussed the influence of the measurement error of the gravity gradiometer on the gravity gradient/inertial integrated navigation system [4].

At present, our country has mastered the kinematics and trajectory planning technology of manipulators, as well as the software and hardware design technology of control system. But on the whole, there is a certain gap between the domestic research level and foreign ones, and the accuracy and reliability are worse than foreign ones. Ekaputra et al. believed that even if inertial sensors, navigation algorithms, and navigation computers are ideal, there will still be errors in inertial navigation. The source of the errors is the error of Earth's gravity field information used in inertial navigation [5]. Jawale et al. proposed using gravity gradient for matching and positioning. Five independent components in the gravity gradient tensor constitute the matching feature. The gravity gradient measurement can better isolate the influence of carrier acceleration, which is conducive to the realization of dynamic measurement [6]. Noort et al. used the stiffness coefficient to adjust the stiffness of the geometric transformation to be solved, which can better cope with the changes of inertial navigation error and speed error [7]. Kim used cloud atomization technology to convert different levels of physical nodes into virtual machine nodes through the research of fog computing framework [8].

Aiming at the correction of the six-dimensional force/torque sensor in the space environment, this paper proposes a method for online calibration of the six-dimensional force/torque sensor based on the space manipulator joint torque sensor and exerts a series of different effects on each joint through the control commands of the manipulator force, making the mechanical arm in a state of internal force balance. Finally, with the introduction of the wrist force sensor gravity compensation model, in combination with the kinematic equations of the robot arm, the wrist force sensor end gravity compensation algorithm is deduced, the reading is corrected, and the force solution method is adjusted. The robot arm and the tip of the robot arm are obtained accurately. The contact force is finally verified by a simulation to verify the correctness of the gravity compensation algorithm at the load end of the arm mechanical force sensor.

2. Gravity Compensation Algorithm and Simulation of Load End of Manipulator Wrist Force Sensor

2.1. Calibration Method of Manipulator Wrist Force Sensor Based on Neural Network. Due to the design and manufacturing of the sensor, there is a mutual coupling between the output signal of the sensor and the actual six-dimensional component force. This interference is very complicated and difficult to accurately describe in theory. It restricts the measurement accuracy of the multidimensional wrist force sensor. One of the main factors [9, 10] is to adopt signal processing methods to eliminate or suppress the coupling between sensor dimensions. This method can not only reduce the requirements on the sensor manufacturing process but also obtain more accurate measurement results. In factor analysis, the weight of each main factor is not determined, but is determined by the relevant variables that affect the changes of these factors.

2.1.1. Linear Calibration of Manipulator Wrist Force Sensor Based on Least Square Method. With certain performance improvements, there are new requirements for general adaptability and specific adaptability. The main problem with basketball gymnastics in Japan is that there are too many regular gymnastics, special gymnastics are not covered, and the obtained physical condition cannot be used for special gymnastics. Suppose F is the input force vector, V is the output voltage vector, and H is the coupling matrix [11, 12], for the mechanical arm wrist force sensor:

$$V = HF. \tag{1}$$

The following transformation is made to the formula:

$$H^T V = \left(H^T H\right) F. \tag{2}$$

We get

$$F = \left(H^T H\right)^{-1} H^T V. \tag{3}$$

Then, we do the following:

$$C = \left(H^T H\right)^{-1} H^T. \tag{4}$$

We call C the calibration matrix. So there are

$$F = CV. \tag{5}$$

When the calibration matrix C is known, for the direct output type manipulator wrist force sensor, the expression is

$$\begin{bmatrix} F_x \\ F_y \\ F_z \end{bmatrix} = \begin{bmatrix} c_{11} & c_{12} & c_{13} \\ c_{21} & c_{22} & c_{23} \\ c_{31} & c_{32} & c_{33} \end{bmatrix} \begin{bmatrix} V_1 \\ V_2 \\ V_3 \end{bmatrix}. \tag{6}$$

In the calculation process of (5), the interdimensional decoupling of the mechanical arm wrist force sensor is also completed. It can be seen that the key to the calibration of the entire sensor is to obtain the calibration matrix C.

Human motion tracking based on template matching currently primarily uses error metrics between two matching pixel blocks. There are three main error metrics based on block matching. An error metric is based on a cross-correlation function and a normalized mean square. When the number of force vectors is equal to the number of output channels, the transfer coefficient matrix can be obtained as [13, 14]

$$C = FV^{-1},$$
$$C = FV^{T}\left(VV^{T}\right)^{-1}. \tag{7}$$

2.1.2. Nonlinear Calibration of Manipulator Wrist Force Sensor Based on BP Neural Network. (1) Artificial Neural Networks. Artificial neuron is the simplification and simulation of biological neuron, and it is the basic processing unit of neural network system. The input and output relationship can be described as

$$y_i = f\left(\sum_{j=1}^{n} w_{ij}u_j - \theta_i\right). \tag{8}$$

We make

$$x_i = \sum_{j=1}^{n}\left(w_{ij}\theta_j - \theta_i\right). \tag{9}$$

Then, there are

$$y_i = f\left(x_i\right). \tag{10}$$

Different types of activation functions can be selected to obtain different types of neuron models. If $-\theta_i$ is regarded as the weight corresponding to the input quantity u_0 which is always equal to 1, then (8) can be written as

$$y_i = f\left(x_i\right) = f\left(\sum_{j=0}^{n} w_{ij}u_j\right). \tag{11}$$

Among them, $w_{i0} = -\theta_i, u_0 = 1$. The output performance of the artificial neuron and even the neural network model is related to the form of the activation function. Therefore, when constructing the neural network model to solve different problems, you should choose the appropriate activation function [15, 16], as shown in (12) and (13). We have the following:

$$f\left(x\right) = \tanh\left(x\right) = \frac{1}{1 + \exp\left(-\beta x\right)}, \quad \beta > 0, \tag{12}$$

$$f\left(x\right) = \tanh\left(x\right) = \frac{1 - \exp\left(-\beta x\right)}{1 + \exp\left(-\beta x\right)}, \quad \beta > 0. \tag{13}$$

The maximum communication delay that the user can tolerate under the cloud and fog architecture is guaranteed, and the user's request is processed within the acceptable communication delay. Therefore, in order to judge whether the manipulator is singular, it is first necessary to determine the Jacobian matrix of the manipulator and then judge whether it is a singular state according to the Jacobian matrix [17].

(2). BP Neural Network. Therefore, it is of theoretical and practical importance for the application of the particle swarm algorithm to generate the initial particle swarm in an appropriate manner. The single-particle tree structure coding design emphasizes the connection between upstream and downstream in the supply chain network. Each node in the network has a unique neuron structure, and its activation function usually uses a sigmoid function, but there is also a linear activation function at the output level [18, 19]. Its structure is shown in Figure 1.

Suppose that in a given sample pair of group L, the sample input u_p and output d_p of group p are

$$u_p = \left(u_{1p}, u_{2p}, \ldots, u_{np}\right), d_p = \left(d_{1p}, d_{2p}, \ldots, d_{np}\right),$$
$$p = 1, 2, \ldots, L. \tag{14}$$

The output of node i when inputting p sample is

$$y_{ip}\left(t\right) = f\left[u_{ip}\left(t\right)\right] = f\left[\sum_{j} w_{ij}\left(t\right)I_{jp}\right]. \tag{15}$$

Among them, I_{jp} represents the j input of node i when the p sample is input; $f\left(\cdot\right)$ represents the differentiable S type activation function. According to (15), starting from the input layer and deducing layer by layer, the output of the nodes of the network output layer can be obtained. Suppose E_p is the objective function of the network when the p sample is input and the L_2 norm is taken; then

$$E_p\left(w, t\right) = \frac{1}{2}\left\|d_p - y_p\left(t\right)\right\|_2^2 = \frac{1}{2}\sum_{k}\left[d_{kp} - y_{kp}\left(t\right)\right]^2,$$
$$= \frac{1}{2}\sum_{k} e_{kp}^2\left(t\right). \tag{16}$$

where $y_{kp}\left(t\right)$ represents the output of the k node in the output layer when the p group of samples are input after the t weight adjustment; $e_{kp}\left(t\right)$ represents the error between the output of the k node of the output layer and the expected output when the p group of samples are input after t weight adjustments. Therefore, the overall objective function of the network is

$$J\left(w, t\right) = \sum_{p} E_p\left(w, t\right), \tag{17}$$

if

$$J\left(w, t\right) \le \varepsilon. \tag{18}$$

Then, the network training ends; otherwise, taking formula (17) as the objective function, the $t + 1$ adjustment formula of the connection weight of neuron j to neuron i can be obtained by the gradient descent method:

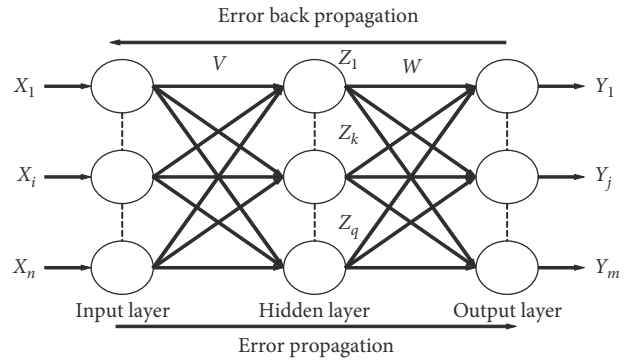

Figure 1: Neural network structure model based on BP algorithm.

$$w_{ij}(t+1) = w_{ij}(t) + \Delta w_{ij}(t),$$
$$\Delta w_{ij} = -\eta \sum_{p} \frac{\partial E_p(w,t)}{\partial w_{ij}(t)}. \tag{19}$$

Here, η is the step size factor, which is called the learning operator here.

2.2. Load Balancing Algorithm

2.2.1. Load Balancing Technology. Load balancing technology uses different methods and technical means to make the equipment in the system more fully function, improve data processing capacity and throughput, and build a network with better flexibility and wider availability. When the load is small, the significance of load balancing is not great. As the load increases, the role of load balancing technology will be clearly seen [20, 21]. Load balancing technology effectively solves the problem of network congestion, improves node utilization, network server response speed, and maintainability, avoids point-to-point network failures, significantly accelerates user access speed and efficiency, and improves system performance.

2.2.2. Load Balancing Technology Classification. The economic environment is the most basic environment. It is the basis for the survival of the financial system and determines the degree of development of the financial system. The financial system was created after economic growth reached a certain level and developed simultaneously with economic growth. The operation of the software must consume part of the system resources, and as the processing load increases, the software itself consumes a large amount of system resources [22, 23]. Global load balancing can achieve geographic independence and schedule tasks on server groups with different network structures. It is used to locate the nearest server through the user's IP address and can also be used for uniform resource allocation. This method can effectively prevent server point failures and network congestion and improve user access efficiency.

2.2.3. Common Load Balancing Algorithms. The law must be able to effectively protect the interests of investors and creditors, to contribute to the establishment and maintenance of good economic order, and thus to ensure the smooth and efficient operation of the financial system. A well-developed credit system can not only effectively reduce the cost of information collection but also reduce the negative choice and moral hazard caused by information asymmetry and reduce the occurrence of financial gaps and financial crises. Servers with different performance have different weights, so that servers with better performance can get more user requests. This algorithm can perform task scheduling according to the processing capacity of the server and reduce the uneven load distribution caused by the difference in the processing capacity of the server [24, 25]. Each load balancing algorithm has certain advantages and disadvantages. Some are suitable for specific scenarios, some are simple to implement, and some have good load balancing effects but higher system overhead and higher cost. By proposing some improvements to existing load balancing algorithms, better load balancing effects can often be achieved.

3. Experimental Design of Gravity Compensation Algorithm for Load End of Manipulator Wrist Force Sensor

3.1. Simulation Platform Construction. After the model is imported into the Adams software, the quality and material parameters of each part need to be set to keep the parameters consistent with the real robot arm. The coordinate system where the center point of the robot arm base is located is the base coordinate system, and the robot arm base is fixed on the ground with a fixed pair. The six joints of the robotic arm are all connected by rotating joints, and other mechanisms are connected by fixed pairs. In this way, the constraint relationship between every two parts of the robotic arm is defined to ensure the correct movement of the robotic arm.

3.2. Data Sources. There are many factors that cause the zero drift of the sensor, mainly two factors, time and temperature. In order to measure the impact of time on the zero point of the sensor, it can be expressed by stability or zero-point drift. Zero-point drift refers to the sensor zero-point drift caused by time. This article first conducts an output voltage experiment on the static performance and coupling error of the mechanical arm wrist force sensor and, secondly, in order to study the influence of temperature changes in the space environment on the zero-point output of the mechanical arm sensor. A high- and low-temperature test box was used to simulate the temperature drift caused by temperature changes to the sensor, and these experimental data were collected for subsequent experimental analysis.

3.3. Experimental Method. The torque information detected by the hinge torque sensor is used as standard force/torque information, which is then converted to the standard power load applied to the six-dimensional force/torque sensor via

Table 1: Data sheet of evaluation index system for index reliability testing.

	Very clear	Clear	General	Not clear	Chaotic	Alpha
Poisson ratio	0.317	0.358	0.174	0.093	0.058	0.9064
Elastic limit	0.294	0.261	0.203	0.166	0.096	0.8433
Yield strength	0.254	0.284	0.189	0.177	0.086	0.8169
Tensile strength	0.242	0.266	0.192	0.174	0.126	0.7672
Linear expansion coefficient	0.237	0.218	0.214	0.194	0.137	0.7394

the Jacobian force. In addition, the voltage signal of the six-dimensional power/torque sensor is collected simultaneously with the output information, and then the minimum quadratic method can be used to perform the electronic calibration of the six-dimensional power/torque sensor. The hinge torque can be used as the standard power sensor, so the hinge torque sensor can be considered to be used to calibrate the robotic arm's six-dimensional force/torque sensor on the web.

3.4. Statistical Data Processing Method. SPSS23.0 software was used for data processing, and count data was expressed as percentage (%), k is the number of data in this experiment, σ^2 is the variance of all survey results, and $P < 0.05$ indicates that the difference is statistically significant. The formula for calculating reliability is shown in the following:

$$a = \frac{k}{k-1}\left(1 - \frac{\sum \sigma_i^2}{\sigma^2}\right). \tag{20}$$

4. Gravity Compensation Algorithm for Load End of Manipulator Wrist Force Sensor

4.1. Index Reliability Test and Patient Condition Analysis. The α coefficient above 0.8 indicates that the effect of index setting is very good, and that above 0.7 is also acceptable. Here, we analyze the reliability of each type of object, and the reliability index we choose for each type of object is slightly different. The results are shown in Table 1.

It can be seen from Figure 2 that the data obtained from Poisson's ratio, elastic limit, yield strength, tensile strength, and linear expansion coefficient of the material has an acceptable impact on this experiment ($\alpha > 0.7$). From this, it can be seen that the properties of the materials used in the robotic arm are sufficient to meet the needs of this experiment and provide a basis for subsequent experiments.

4.2. Based on the Static Performance and Coupling Error of the Sensor

4.2.1. Analysis of Various Static Performance Indicators Based on Sensors. Through the processing of the experimental data of loading and unloading in each direction of the sensor, and using the least square method to decouple the sensor, the static performance indicators of the sensor are analyzed here (Table 2).

It can be seen from Figure 3 that the linearity of the sensor is less than 2%, the maximum linearity is 1.93% in the Mx direction, the minimum linearity is 0.45% in the Fx direction, the maximum repeatability error is 1.43% in the Fz direction, the smallest the repeatability error is 0.94% in the Fx direction, the stability of the sensor is good, the maximum stability error is 0.93% in the My direction, the maximum hysteresis characteristic of the sensor is 1.09% in the Fz direction, and the smallest hysteresis characteristic is 0.56 in the My direction %.

4.2.2. Analysis Based on the Coupling Error of the Sensor. Through the processing of the experimental data of loading and unloading in each direction of the sensor, and using the least square method to decouple the sensor, the coupling error of the sensor is analyzed here, and the results are shown in Table 3.

It can be seen from Figure 4 that the maximum coupling error in the Fx direction is 0.93%, the maximum coupling error in the Fy direction is 0.71%, the maximum coupling error in the Fz direction is 1.81%, the maximum coupling error in the Mx direction is 0.76%, the maximum coupling error in the My direction the error is 1.31%, the maximum coupling error in the Mz direction is 1.33%, and the maximum coupling error of the sensor is 1.81%, which is less than 2% of the design index, so it meets the requirements.

4.3. Temperature Drift Characteristics of Wrist Force Sensor Based on Manipulator

4.3.1. Sensor Temperature Drift Experiment. Assume that the sensor's zero-point drifts due to temperature changes, and the phenomenon that causes the sensor to have a force output is the temperature drift of the sensor. In this paper, the false output force output by the sensor zero-point change caused by temperature drift is defined as temperature drift force, and the results are shown in Table 4.

The collected output voltage signal vector of each sampling point of the sensor caused by temperature change is compared and analyzed, and the temperature drift force can be obtained by using the sensor calibration matrix obtained by static calibration. It is found that the temperature changes will have a great impact on the sensor, among which Fy and Fz have the greatest impact. The specific situation is shown in Figure 5. When the number of partners is small, the degree of new and old model in relation to the optimal solution is not obvious. When the number of partners is large, the new model's model optimization effect is slightly reduced. As the number of partners gradually increased, the degree of optimization of the new model compared to the old model became more and more evident ($P < 0.05$).

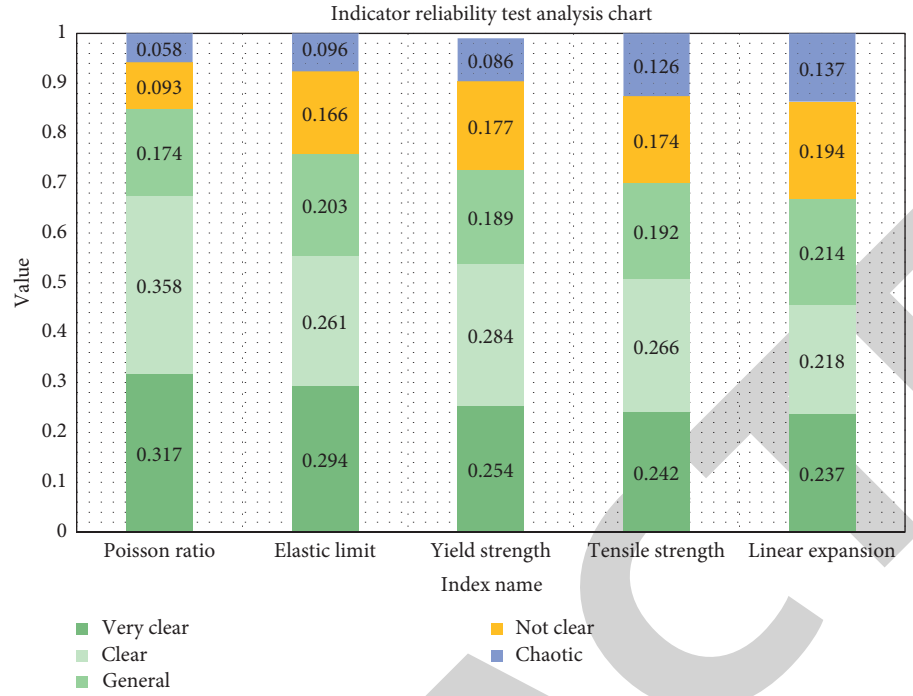

Figure 2: Indicator reliability test analysis chart.

Table 2: The static performance of F/T sensor.

Index	Fx (%)	Fy (%)	Fz (%)	Mx (%)	My (%)	Mz (%)
Linearity	0.45	0.56	0.57	1.93	0.82	1.53
Repeatability	0.94	1.01	1.43	1.32	1.39	1.18
Stability	0.63	0.77	0.79	0.81	0.93	0.68
Hysteresis	0.71	0.61	0.84	1.09	0.56	0.84
Accuracy	1.27	0.82	1.57	1.33	1.36	1.54

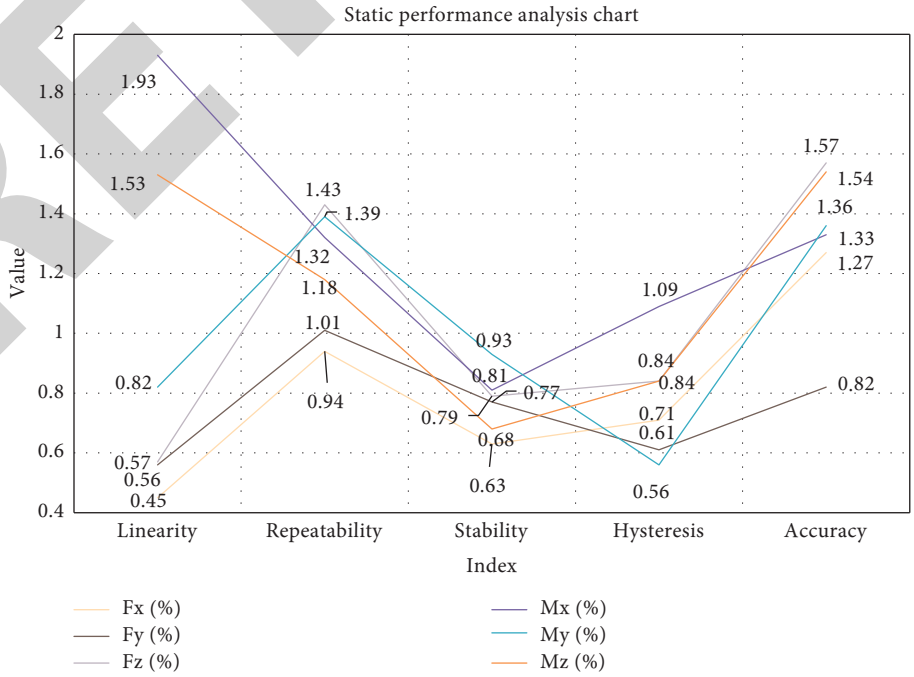

Figure 3: The static performance analysis chart of the sensor.

Table 3: The coupling error of F/T sensor.

Applied force/moment	Fx (%)	Fy (%)	Fz (%)	Mx (%)	My (%)	Mz (%)
Fx	0.75	0.19	1.43	0.23	0.75	1.04
Fy	0.93	0.75	1.81	0.32	0.12	1.33
Fz	0.86	0.43	0.75	0.76	0.74	0.29
Mx	0.73	0.22	1.51	0.75	1.31	0.14
My	0.18	0.27	0.81	0.16	0.75	0.36
Mz	0.61	0.71	0.63	0.57	0.72	0.75

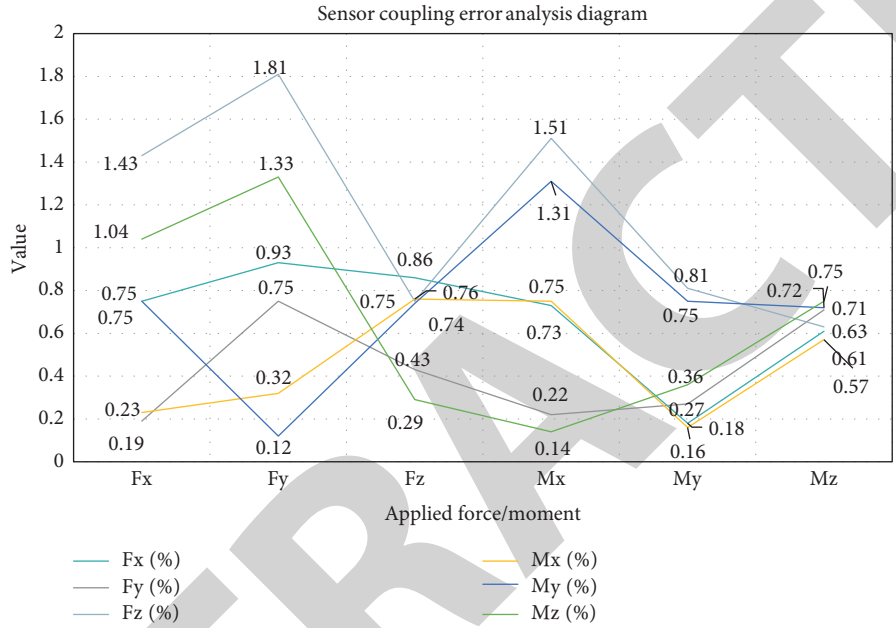

Figure 4: Sensor coupling error analysis diagram.

Table 4: The force caused by temperature drift in each sample.

Temperature (°C)	Fx	Fy	Fz	Mx	My	Mz
−20	1.01	1.68	1.73	2.18	2.47	2.57
−10	1.44	1.50	1.65	2.14	2.48	2.42
0	1.27	1.62	1.97	1.78	2.09	2.65
10	1.30	1.30	1.82	2.15	2.18	2.70
20	1.20	1.34	1.99	2.29	2.33	2.71
30	1.23	1.32	1.75	2.24	2.48	2.83
40	1.11	1.58	1.67	2.22	2.31	2.62
50	1.10	1.36	1.51	2.02	2.08	2.81

4.3.2. Research on Sensor Temperature Drift Compensation Based on Least Square Method. In order to quantify the influence of temperature drift on the force or torque in each direction of the sensor, the author defines the temperature drift error, which can be expressed as the force or torque caused by temperature divided by the rated force or torque of each dimension, and the results are shown in Table 5. Show.

As the temperature increases, the temperature drift error of Fx remains basically unchanged, and the temperature drift error of Fy and Mx gradually decreases from a positive value to zero and then changes to a negative value. The temperature drift errors of Fz, My, and Mz gradually increase from a negative value to zero and then continue to increase to a positive value. It shows that the effect of temperature drift on Fx is almost negligible, and the effect of temperature drift on Mx and Mz is similar, except that the positive and negative characteristics are opposite. The maximum temperature drift errors of Fx, Mx, and Mz are all less than 2%. The maximum temperature drift errors of My, Fy, and Fz are all greater than 2%, as shown in Figure 6.

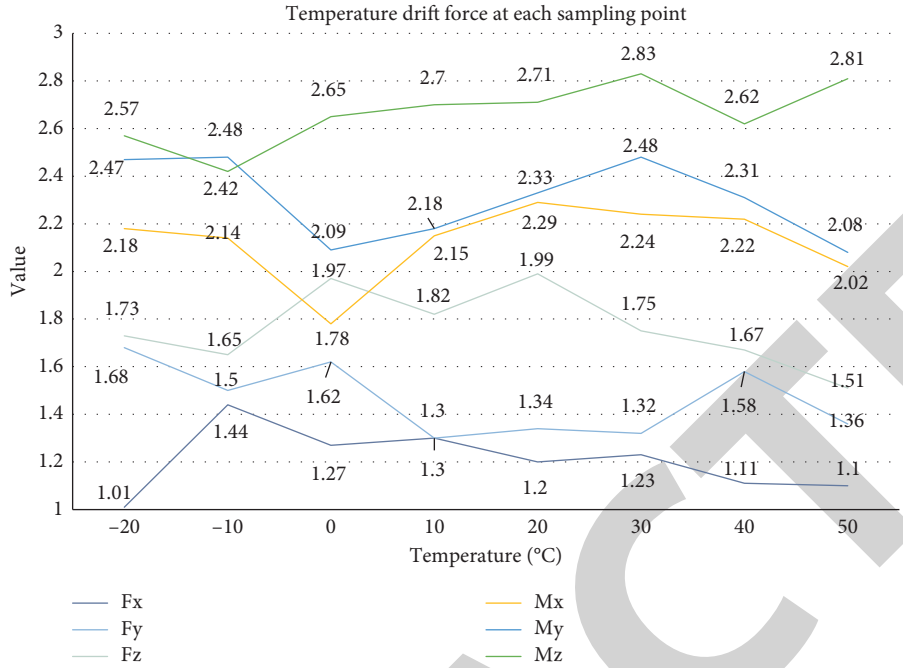

Figure 5: Analysis graph of temperature drift force at each sampling point.

Table 5: The temperature drift error in each sample.

Temperature (°C)	Fx	Fy	Fz	Mx	My	Mz
−20	0.3	8.7	−16.9	2.3	−6.7	−3.7
−10	−0.3	6.4	−11.6	1.8	−4.4	−3.1
0	0.1	4.6	−8.4	1.3	−3.2	−2.5
10	0.3	3.5	−3.7	0.8	−2.6	−2.1
20	0.3	0.7	0.4	0.3	−0.9	−0.8
30	0.4	−1.9	4.6	−0.2	0.5	0.2
40	0.6	−4.3	8.1	−0.7	1.6	1.1
50	0.8	−6.2	10.3	−1.1	2.5	1.9

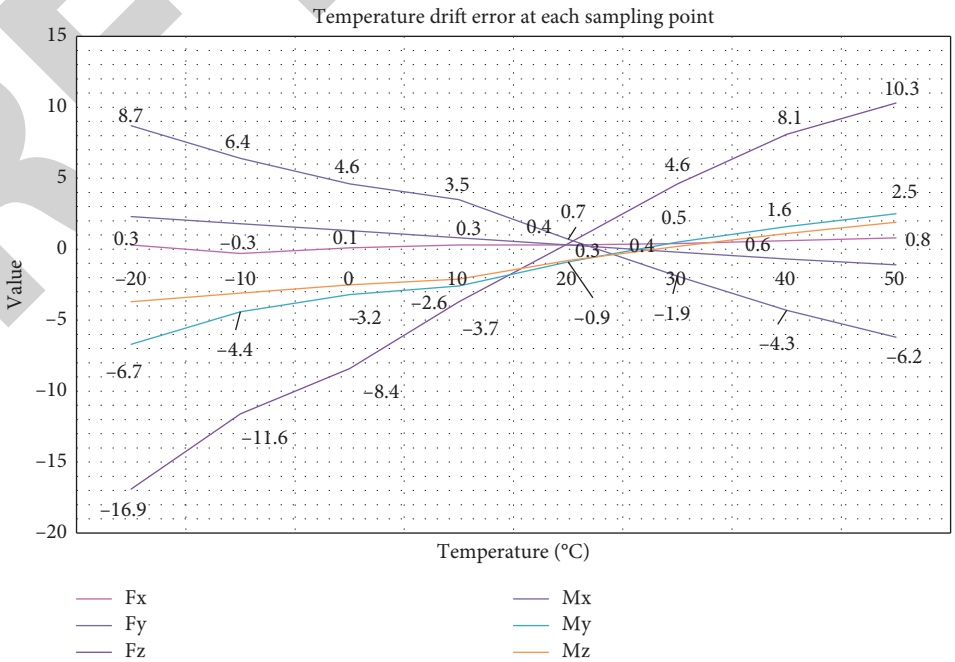

Figure 6: Analysis graph of temperature drift error at each sampling point.

Table 6: The temperature drift error compensated by RBF neural network.

Temperature (°C)	Fx	Fy	Fz	Mx	My	Mz
−20	1.21	1.62	1.57	2.26	2.04	2.41
−10	1.36	1.69	1.97	2.24	2.12	2.9
0	1.24	1.61	1.73	1.93	2.37	2.68
10	1.11	1.32	1.90	1.93	2.50	2.64
20	1.37	1.35	1.92	1.88	2.42	2.61
30	1.46	1.41	1.53	2.06	2.05	2.68
40	1.45	1.49	1.68	2.26	2.05	2.59
50	1.02	1.46	1.79	1.90	2.32	2.64

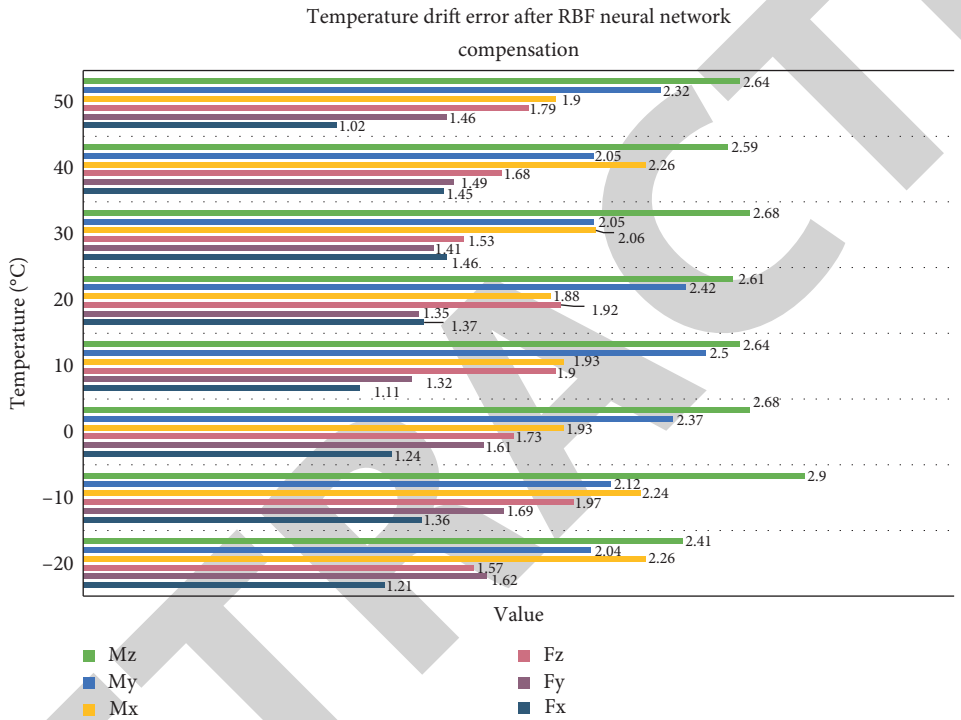

Figure 7: Analysis of temperature drift error after RBF neural network compensation.

4.3.3. Analysis Based on Initial Indicators. The temperature drift error of the sensor after temperature compensation through the RBF network is shown in Table 6.

After compensation, the temperature drift error of Fx is greater than 0.08% and less than 0.5%; the temperature drift error of Fy is greater than 0.1% and less than 0.25%; the temperature drift error of Fz is greater than 0.25% and less than 0.6%; the temperature drift error of Mx is greater than 0.25% and less than 0.5%; the temperature drift error of My is greater than 0.1% and less than 0.5%; the temperature drift error of Mz is greater than 0.1% and less than 0.25%, as shown in Figure 7.

5. Conclusions

The influence of the behavior change of the operator terminal load on the zero value of the six-dimensional force sensor and the gravity and center of gravity position of the operator terminal load can be obtained through experimental methods. The wrist force gravity tip load algorithm and the operator's end force calculation method create a model of the wrist force sensor gravity compensation system. When reading the six-dimensional force sensor on the wrist, this method solves the effect of excessive gravity on the load end of the robotic arm. When the operator is in a variable stop motion with low angular acceleration, in principle, the inertia during the motion can be ignored, and the influence of gravity on the load end of the power sensor can be eliminated. The simulation proves the effectiveness of this method and can be widely used based on power feedback and other heavy industrial robots in similar operating environments.

Due to the very complex structure of the six-dimensional force/torque sensor's sensitive components, it is impossible to obtain accurate theoretical expressions. Although the results of finite element analysis are more accurate, the amount of calculation is very large, and the sensor model with the best performance is often not available. Regarding the disadvantages, the sensor is used to detect the force and moment that the end manipulator of the space manipulator

bears when interacting with the external environment and provides necessary force sensing information for the force control and compliant motion control of the manipulator, so as to complete some complex and delicate tasks. It is an important condition to realize the intelligentization of the space manipulator. In this article, the author proposes a response surface method to obtain an approximate mathematical model of the sensor's sensitive components and then, based on the fitted response surface model, use the minimum condition number of the sensor strain compliance matrix as the optimization goal.

In order to obtain the static characteristics of the arm wrist mechanical force sensor, a calibration system based on the pulley weight is designed and the calibration system error is analyzed. The calibration matrix of the arm mechanical strength sensor is obtained with the minimum square method, and various static performance indicators and sensor connection errors are obtained through loading and unloading experiments. In order to change the sensor temperature, a compensation method is proposed based on optimizing the particle velocity optimization based on a square support carrier machine. A basic mechanical analysis was performed on the operator and the operator's tendency to change the driving force and the constant variation of the force of each joint when the operator was held was determined. The power of the operator was analyzed, and the material was determined to meet the strength requirements.

Data Availability

No data were used to support this study.

Conflicts of Interest

The authors declare that they have no conflicts of interest.

References

[1] B. Sprowl, "AI robotic arm gets experience cooking fried chicken and tater tots," *Unmanned Systems*, vol. 36, no. 8, p. 52, 2018.

[2] K. Ahlin, B. Joffe, A.-P. Hu, G. McMurray, and N. Sadegh, "Autonomous leaf picking using deep learning and visual-servoing," *IFAC-PapersOnLine*, vol. 49, no. 16, pp. 177–183, 2016.

[3] M. C. Cuervo, "Joint amplitude MEMS based measurement platform for low cost and high accessibility telerehabilitation: elbow case study," *Journal of Bodyward Movement Therapies*, vol. 21, no. 3, pp. 574–581, 2017.

[4] M. Farman, M. Al-Shaibah, Z. Aoraiath, and F. Jarrar, "Design of a three degrees of freedom robotic arm," *International Journal of Computer Applications*, vol. 179, no. 37, pp. 12–17, 2018.

[5] I. M. Ekaputra, J. D. Setiawan, and J. Setiawan, "Pengembangan wearable robotic arm input dan virtual instrument untuk pengendalian dan pemantauan lengan robot," *Jurnal Rekayasa Mesin*, vol. 8, no. 2, pp. 109–119, 2017.

[6] H. P. Jawale, A. Jaiswal, and K. N. Bhasme, "Design and analysis of three-axis cantilever type force sensor," *World Journal of Engineering*, vol. 16, no. 4, pp. 497–508, 2019.

[7] J. C. V. D. Noort, R. Verhagen, K. J. V. Dijk et al., "Quantification of hand motor symptoms in Parkinson's disease: a proof-of-principle study using inertial and force sensors," *Annals of Biomedical Engineering*, vol. 45, no. 10, pp. 2423–2436, 2017.

[8] G.-S. Kim, "Development of a wrist bending rehabilitation robot with a three-axis force sensor," *Journal of Sensor Science and Technology*, vol. 25, no. 1, pp. 27–34, 2016.

[9] C. Bals, "Toward a supply chain finance (SCF) ecosystem - proposing a framework and agenda for future research," *Journal of Purchasing and Supply Management*, vol. 25, no. 2, pp. 105–117, 2019.

[10] Y. Du and Q. Zhu, "Decentralized adaptive force/position control of reconfigurable manipulator based on soft sensors," *Proceedings of the Institution of Mechanical Engineers, Part I: Journal of Systems and Control Engineering*, vol. 232, no. 9, pp. 1260–1271, 2018.

[11] R. Azzi, R. K. Chamoun, and M. Sokhn, "The power of a blockchain-based supply chain," *Computers & Industrial Engineering*, vol. 135, no. SEP, pp. 582–592, 2019.

[12] S. Fldi, T. Horváth, F. Zieger et al., "A novel non-invasive blood pressure waveform measuring system compared to Millar applanation tonometry," *Journal of Clinical Monitoring and Computing*, vol. 32, no. 4, pp. 717–727, 2018.

[13] J. Wang, G. Zuo, J. Zhang et al., "Research on assist-as-needed control strategy of wrist function-rehabilitation robot," *Journal of Biomedical Engineering*, vol. 37, no. 1, pp. 129–135, 2020.

[14] A. Mancisidor, A. Zubizarreta, I. Cabanes, P. Bengoa, and J. H. Jung, "Kinematical and dynamical modeling of a multipurpose upper limbs rehabilitation robot," *Robotics and Computer-Integrated Manufacturing*, vol. 49, no. feb, pp. 374–387, 2018.

[15] S. Zhang, S. Guo, B. Gao et al., "Muscle strength assessment system using sEMG-based force prediction method for wrist joint," *Journal of Medical and Biological Engineering*, vol. 36, no. 1, pp. 121–131, 2016.

[16] G. I. Zamora-Gómez, A. Zavala-Río, D. J. López-Araujo, E. Nuño, and E. Cruz-Zavala, "An output-feedback global continuous control scheme with desired gravity compensation for the finite-time and exponential regulation of bounded-input robotic systems," *IFAC-PapersOnLine*, vol. 51, no. 22, pp. 108–114, 2018.

[17] Q. H. Wang, S. C. Wu, J. W. Liu, and J. R. Li, "Design of a 6-DOF force device for virtual assembly (FDVA-6) of mechanical parts," *Mechanics Based Design of Structures and Machines*, vol. 46, no. 5, pp. 567–577, 2018.

[18] G. Feng, Q. ChenKun, A Y Ren, and X. Zhao, "Hardware-in-the-loop simulation for the contact dynamic process of flying objects in space," *Science China Technological Sciences*, vol. 59, no. 8, pp. 1167–1175, 2016.

[19] Y. He, F. Zhang, M. Yang et al., "Design of tracking suspension gravity compensation system for satellite antenna deployable manipulator," *Jiqiren/Robot*, vol. 40, no. 3, pp. 377–384, 2018.

[20] Z. Zhu, J. Yuan, J. Song, and R. Cui, "An improving method for micro-G simulation with magnetism-buoyancy hybrid system," *Advances in Space Research*, vol. 57, no. 12, pp. 2548–2558, 2016.

[21] D. Lee, S. Lee, J. Park, and T. Seo, "Novel gravity compensation mechanism by using wire-winding," *Journal of Institute of Control, Robotics and Systems*, vol. 22, no. 9, pp. 733–737, 2016.

[22] P. Ni, W. Zhang, X. Zhu et al., "Learning an end-to-end spatial grasp generation and refinement algorithm from simulation," *Machine Vision and Applications*, vol. 32, no. 1, pp. 1–12, 2021.

[23] S. M. Farzam and A. A. Khan, "A novel Local Time Stepping algorithm for shallow water flow simulation in the discontinuous Galerkin framework - ScienceDirect," *Applied Mathematical Modelling*, vol. 40, no. 1, pp. 70–84, 2016.

[24] N. Tajbakhsh, J. Y. Shin, S. R. Gurudu et al., "Convolutional neural networks for medical image analysis: full training or fine tuning?" *IEEE Transactions on Medical Imaging*, vol. 35, no. 5, pp. 1299–1312, 2016.

[25] Z. Z. Quancong, Z. Wu, Z. Cao, Q. Jiang, and Z. Hua, "Simulation and heat exchanger network designs for a novel single-column cryogenic air separation process," *Chinese Journal of Chemical Engineering*, vol. 27, no. 07, pp. 47–58, 2019.